Detecting activity-evoked pH changes in human brain

Vincent A. Magnotta[a,b,1], Hye-Young Heo[a], Brian J. Dlouhy[c], Nader S. Dahdaleh[c], Robin L. Follmer[b], Daniel R. Thedens[a], Michael J. Welsh[c,d,e,f,g,h,1], and John A. Wemmie[b,c,e,f,h,i,1]

Departments of [a]Radiology, [b]Psychiatry, [c]Neurosurgery, [d]Internal Medicine, and [e]Molecular Physiology and Biophysics, [f]Interdisciplinary Graduate Program in Neuroscience, [g]Howard Hughes Medical Institute, and [h]Roy J. and Lucille A. Carver College of Medicine, University of Iowa, Iowa City, IA 52242; and [i]Department of Veterans Affairs Medical Center, Iowa City, IA 52242

Contributed by Michael J. Welsh, April 10, 2012 (sent for review February 28, 2012)

Localized pH changes have been suggested to occur in the brain during normal function. However, the existence of such pH changes has also been questioned. Lack of methods for noninvasively measuring pH with high spatial and temporal resolution has limited insight into this issue. Here we report that a magnetic resonance imaging (MRI) strategy, T_1 relaxation in the rotating frame ($T_1\rho$), is sufficiently sensitive to detect widespread pH changes in the mouse and human brain evoked by systemically manipulating carbon dioxide or bicarbonate. Moreover, $T_1\rho$ detected a localized acidosis in the human visual cortex induced by a flashing checkerboard. Lactate measurements and pH-sensitive ^{31}P spectroscopy at the same site also identified a localized acidosis. Consistent with the established role for pH in blood flow recruitment, $T_1\rho$ correlated with blood oxygenation level-dependent contrast commonly used in functional MRI. However, $T_1\rho$ was not directly sensitive to blood oxygen content. These observations indicate that localized pH fluctuations occur in the human brain during normal function. Furthermore, they suggest a unique functional imaging strategy based on pH that is independent of traditional functional MRI contrast mechanisms.

brain pH | functional magnetic resonance imaging | T1rho

To what degree pH changes during normal brain function is unclear (1). However, neuronal activity could cause transient, localized pH changes via several mechanisms. Increased neuronal activity enhances carbohydrate metabolism producing the pH-lowering by-products lactic acid and CO_2 (2). Activity-evoked HCO_3^- transport can alter pH (3). Local field potentials produced by ion fluxes could change pH (4). In addition, acidic synaptic vesicles release protons during neurotransmission (5). Such dynamic pH fluctuations have the potential to dramatically alter physiology and behavior through a number of pH-sensitive receptors and channels (6). Acid-sensing ion channels, for example, play critical roles in synaptic plasticity, learning, memory, pain, and neurodegeneration (7–10). Superimposed on activity-dependent brain pH changes and the potential physiological effects are several buffering systems. Principal among these is the CO_2/HCO_3^- system. In a reversible reaction, CO_2 combines with water to form carbonic acid, which readily dissociates into HCO_3^- and H^+. Raising HCO_3^- shifts the equilibrium away from H^+ and increases pH. Conversely, raising CO_2 shifts the equilibrium toward H^+, thereby lowering pH. The ability to measure these pH changes in the functioning brain is key for gaining insight into this poorly understood dimension of CNS physiology and pathophysiology.

Routinely measuring pH in the brain would require novel noninvasive methods. Traditionally, ^{31}P spectroscopy has been used to estimate brain pH (11); however, ^{31}P is limited by poor spatial resolution (typically 10- to 30-cm^3 volumes), long acquisition times (often 5–10 min for a single measurement), and the need for special hardware not typically available on clinical scanners. Recently, ^{1}H MRI pulse sequences have been shown to detect H^+ exchange between water and proteins and thus can be highly pH sensitive. These techniques include amide proton transfer (APT) and T_1 in the rotating frame ($T_1\rho$) (12–15). APT detects H^+ exchange by taking advantage of differences in resonances between amide and water protons. The spin-lock preparation pulse used in $T_1\rho$ imaging sensitizes the magnetic resonance (MR) signal to relaxation effects arising from H^+ exchange between free water protons and those bound to proteins and macromolecules. Here, we focused on $T_1\rho$ because of its pH sensitivity, high spatial and temporal resolution, and potential to detect dynamic pH changes during brain function.

Results

Validation of pH Sensitivity in Buffered Phantoms. To evaluate $T_1\rho$ sensitivity to pH in the physiological range, we first studied phantoms [3.5% agar (wt/vol)], 8% BSA (wt/vol), 0.1 M phosphate buffered saline pH-adjusted with HCl and NaOH to values ranging from pH 6.0 to pH 8.0 (Fig. 1*A*). They were imaged by using a fast spin-echo sequence with a spin-locking preparation pulse, which created a B_1 field of 1,000 Hz, and four spin-lock times (10, 20, 40, and 60 ms). $T_1\rho$ times were inversely proportional to the measured pH ($R^2 = 0.98$) (Fig. 1*A*), suggesting that $T_1\rho$ is sensitive to pH in the physiological range.

$T_1\rho$ Insensitivity to Oxyhemoglobin Content. Because current blood oxygenation level-dependent (BOLD) imaging relies on T_2^* contrast to detect changes in blood oxyhemoglobin content, we compared the specificity of $T_1\rho$ and T_2^* for pH and oxygen content in fresh sheep blood. Blood pH and O_2 content were varied in three test conditions: (*i*) unaltered, (*ii*) acidified (25 mM HCl), and (*iii*) oxygenated with 100% O_2. Data from a single axial slice were collected by using a $T_1\rho$ fast spin-echo sequence and T_2^*-weighted gradient-echo sequence. We found that $T_1\rho$ was sensitive to pH, but not O_2 content (Fig. 1*B*). Conversely, T_2^* was sensitive to O_2 content, but not pH (Fig. 1*C*). These data suggest that $T_1\rho$ changes are unlikely due to changes in oxyhemoglobin content.

pH Detection in Mouse Brain. To assess pH sensitivity of $T_1\rho$ in vivo, measurements were simultaneously obtained with $T_1\rho$ and a custom-made MRI-compatible pH sensor (pHOptica; World Precision Instruments; detection range pH 5–9) implanted into the amygdala of mice. Data were collected from anesthetized mice under three conditions: (*i*) room air inhalation, (*ii*) 20% CO_2 inhalation, and (*iii*) following HCO_3^- injection (5 mmol/kg, i.p.). Fig. 2*A* shows examples of $T_1\rho$ maps obtained from a single mouse brain. Direct pH measurements varied from animal to animal, most likely due to differences in respiratory suppression from anesthesia. In all cases, CO_2 inhalation lowered pH relative to air and prolonged $T_1\rho$ times throughout the brain, including at the pH-sensing probe tip. HCO_3^- injection produced the opposite effect, raising pH and shortening $T_1\rho$ times. Fig. 2*B* shows the relationship between $T_1\rho$ at the sensor

Author contributions: V.A.M., D.R.T., M.J.W., and J.A.W. designed research; V.A.M., H.-Y.H., B.J.D., N.S.D., R.L.F., and J.A.W. performed research; V.A.M., H.-Y.H., B.J.D., N.S.D., and J.A.W. contributed new reagents/analytic tools; V.A.M., H.-Y.H., and J.A.W. analyzed data; and V.A.M., B.J.D., N.S.D., R.L.F., M.J.W., and J.A.W. wrote the paper.

The authors declare no conflict of interest.

Freely available online through the PNAS open access option.

[1]To whom correspondence may be addressed. E-mail: vincent-magnotta@uiowa.edu, michael-welsh@uiowa.edu, or john-wemmie@uiowa.edu.

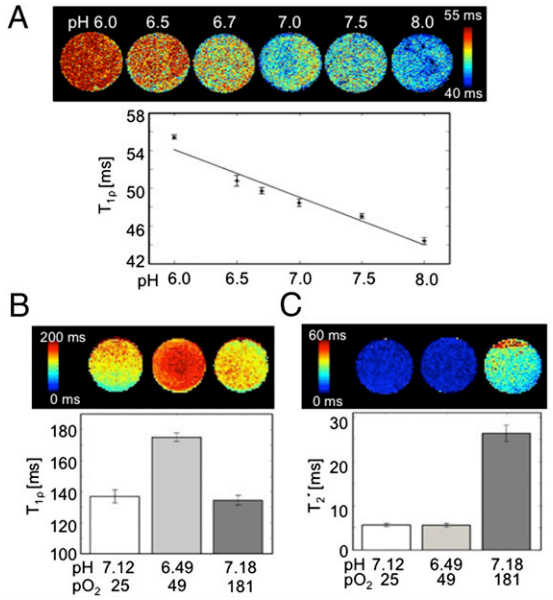

Fig. 1. $T_1\rho$ and T_2* sensitivity to pH and pO_2 manipulations. (*A*) $T_1\rho$ maps for agar phantoms with pH adjusted to different levels (6.0–8.0). The relationship between $T_1\rho$ times and pH was linear within this range. The estimated T_1 times were calculated within a central 5 × 5 region. (*B*) $T_1\rho$ maps in sheep blood phantoms (*Upper*) with corresponding mean and SD in a central 5 × 5 region of interest plotted in *Lower*. The sheep blood phantoms are arranged from left to right as follows: unaltered (control), acidified, and hyperoxygenated. (*C*) Corresponding T_2* maps in same sheep blood phantoms (*Upper*) with mean and SD in a central 5 × 5 region of interest plotted in *Lower*.

tip and pH measured from the sensor across all mice and conditions (R^2 = 0.77).

Systemic pH Changes in Human Brain Induced by CO_2 and Hyperventilation. Qualitatively similar $T_1\rho$ responses were observed in the human brain when pH was manipulated through breathing. A research participant was imaged on a Siemens 3T scanner under three conditions: (*i*) normal breathing of room air, (*ii*) breathing 5% CO_2, and (*iii*) paced hyperventilation of room air (27 breaths per minute). These manipulations changed average end-tidal CO_2 ($EtCO_2$) measurements from 4.3% to 7.7% CO_2 (Fig. 3*B*). Consistent with hypercarbic acidosis, CO_2 inhalation produced a widespread increase in T1ρ relaxation time (Fig. 3 *A* and *B*). Paced hyperventilation produced the opposite effect, and consistent with a respiratory alkalosis reduced $T_1\rho$ times (Fig. 3 *A* and *B*). Fig. 3*C* shows the subtracted $T_1\rho$ maps between hyperventilation and room air, and between 5% CO_2 and room air, suggesting that these systemic manipulations change pH throughout the brain.

Localized pH Changes Induced by Flashing Checkerboard. With the above data suggesting that $T_1\rho$ is sensitive to brain pH, we hypothesized that $T_1\rho$ might detect localized pH changes evoked by brain activation. To test this hypothesis, we used a visual flashing checkerboard task (Fig. 4*A*). Six participants were presented with a visual flashing checkerboard (22 × 22 squares) alternating at 8 Hz in a block design (Fig. 4*A*) (16). For comparison, two runs of BOLD were interleaved with three runs of $T_1\rho$. Fig. 4*B* shows the group activation maps for the $T_1\rho$ and BOLD imaging overlaid on the average T_1-weighted anatomical image. Voxels exhibiting significant activation ($P < 0.05$, corrected) are shown. The flashing checkerboard significantly increased $T_1\rho$ times in the occipital cortex. A similar activation region was measured by functional MRI (fMRI) BOLD. Consistent with the observation that $T_1\rho$ and BOLD detect mutually independent phenomena, a difference was observed between the size of the $T_1\rho$- and BOLD-responsive areas. The reason for this apparent difference is not clear. It is possible that $T_1\rho$ detects more focal changes than BOLD, given that the vascular tree underlying the hemodynamic response is larger than regions of neural activity. For example, venous drainage of brain areas can extend the BOLD signal tens of millimeters from the activation site (17). The well-established effect of acidic pH on blood flow (18) suggests localized acidosis might even help drive the BOLD response.

Because lactic acid is one potential source of localized pH change, we measured lactate by ^{1}H MR spectroscopy (MRS) in a voxel positioned at the BOLD site. Consistent with a previous report (19), we found that the flashing checkerboard significantly

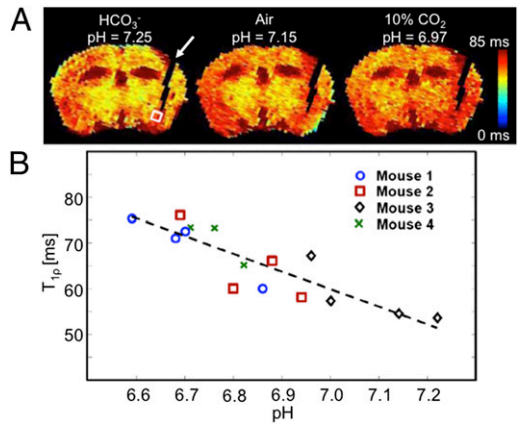

Fig. 2. $T_1\rho$ detects pH changes in the anesthetized mouse brain evoked by CO_2 inhalation or i.p. HCO_3^- injection. (*A*) $T_1\rho$ maps from a mouse brain after given bicarbonate (*Left*), exposed to room air (*Center*), and exposed to 10% CO_2 (*Right*). The position of the fiber-optic pH sensor is shown by the white arrow, and the open square indicates the location of the ROI used for estimating the $T_1\rho$ times. (*B*) The relationship between the mean $T_1\rho$ times and the corresponding direct pH measurements obtained from the fiber-optic sensor across four mice. Each mouse is represented by a different symbol.

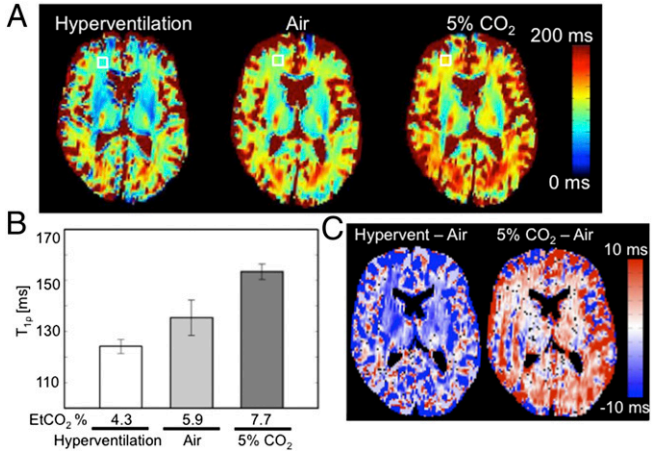

Fig. 3. $T_1\rho$ measurements throughout the human brain are responsive to $EtCO_2$ manipulation. (*A*) $T_1\rho$ maps of the human brain varied with $EtCO_2$ concentration during hyperventilation, breathing room air, and 5% CO_2 challenge. The open box identifies a 7 × 7 region of interest in white matter where $T_1\rho$ time estimates were obtained. (*B*) The estimated $T_1\rho$ times in white matter varied with measured $EtCO_2$ concentrations (module CO2100C; Biopac). (*C*) $T_1\rho$ subtraction images between the hyperventilation and air conditions (*Left*) and 5% CO_2 and air condition (*Right*).

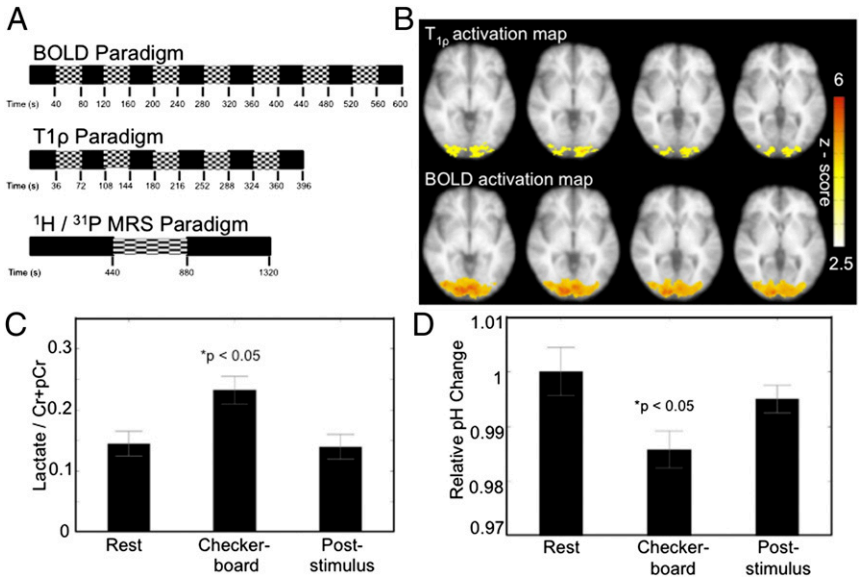

Fig. 4. Flashing checkerboard alters $T_1\rho$, BOLD, lactate, and ^{31}P measurements in the visual cortex. (*A*) Flashing checkerboard paradigms for functional $T_1\rho$, BOLD, and MRS studies. For the $T_1\rho$/BOLD studies, three runs of the $T_1\rho$ block sequence where interleaved with two runs of BOLD. (*B*) $T_1\rho$ and BOLD functional activation maps ($P < 0.05$, corrected) resulting from the visual flashing checkerboard stimulus. Four contiguous slices are shown. (*C*) Lactate to total creatine ratio increased significantly during visual stimulation relative to both baseline and the poststimulus recovery phase. $^*P < 0.05$, paired *t* test. (*D*) ^{31}P spectroscopy estimates of pH in the visual cortex were significantly reduced during flashing checkerboard presentation relative to both baseline and recovery. $^*P < 0.05$, paired *t* test.

increased the lactate-to-creatine ratio (Fig. 4*C*). If the $T_1\rho$ and lactate responses indeed reflect a localized acidosis, we hypothesized that we should be able to detect the pH change with an alternative method. We chose ^{31}P spectroscopy, a widely accepted measure of pH, and used the $T_1\rho$ data to guide voxel positioning. In six additional subjects, the flashing checkerboard altered visual cortex ^{31}P estimates of pH (Fig. 4*D*). Like $T_1\rho$, these changes indicate a transient, activity-dependent localized acidosis.

Discussion

These results indicate that neuronal activity can change local pH in the human brain during normal function. Neuronal activation may lower pH through a variety of processes (20) acting individually or together to produce the acidosis observed here; further study will be required to identify the mechanisms underlying this pH change. Because monocarboxylate transporters cotransport protons with lactate (21), our studies suggest that lactate production and transport might contribute to the localized acidosis.

The localized acidosis observed here might have a number of consequences for brain physiology and pathophysiology (6, 8). The reduced pH could activate some ion channels and receptors and inhibit others, thereby influencing brain function and behavior (5, 7, 8, 22). A reduced pH has also been implicated in ischemic stroke, neurodegenerative disease, seizures, and respiratory control (9, 10, 23–27). Interestingly, in patients with panic disorder, lactate induction by the flashing checkerboard was abnormally elevated (19). Others have also suggested lactate and pH-buffering abnormalities in panic disorder (28). These observations coupled with our findings support the possibility that abnormal pH dynamics may contribute to panic disorder (2).

Additional advances in our knowledge of brain pH dynamics might come from the improved spatial and temporal resolution provided by $T_1\rho$. The $T_1\rho$ sequence used here has an isotropic spatial resolution of ~4 mm and temporal resolution of 6 s, whereas the spatial and temporal resolutions of ^{31}P spectroscopy are 30 mm and several minutes, respectively. Further improvements in the $T_1\rho$ scan time may be possible by acquiring only two spin-lock times and by using parallel imaging. Comparable temporal and spatial resolution might also be possible with APT in an echo-planar sequence if only two frequency-offset pulses were applied about the center imaging frequency.

One limitation of both $T_1\rho$ and APT is that they depend on H^+ exchange with proteins and amide groups. Thus, either $T_1\rho$ or APT could be affected by appreciable changes in local protein concentration as well as pH. The observation that $T_1\rho$ correlated closely with direct pH measurements in the mouse brain and with secondary pH imaging methods in human brain argues that the $T_1\rho$ changes observed here were due at least in part to pH.

In addition to improving the ability to measure brain pH, this study has unique implications for functional imaging in general. Because $T_1\rho$ showed a linear response to pH, $T_1\rho$ may be more quantifiable than BOLD fMRI, which is not quantifiable other than percent change and does not address baseline conditions. In addition, the spatial resolutions of BOLD fMRI and ^{15}O-water positron emission tomography depend on blood flow and oxyhemoglobin content and are thus limited by the vascular anatomy. Although $T_1\rho$ provided a similar pattern of activation as BOLD, $T_1\rho$ changes were independent of blood oxygenation. Thus, by measuring functional pH changes, $T_1\rho$ MRI might provide a means for more precisely localizing brain activity.

Methods

Sheep Blood Phantom Imaging. All animal care met National Institutes of Health standards, and the University of Iowa Animal Care and Use Committee approved all procedures. $T_1\rho$ data were collected by using a fast spin-echo sequence with four spin-lock times (10, 20, 40, and 60 ms) and B_1 = 400 Hz. T_2*-weighted imaging, which is sensitive to blood oxygenation, was obtained from a single axial slice by using a gradient-echo sequence with eight echo-times (1.7, 2, 3, 6, 9, 12, 14, and 16 ms). pH, pO_2, and pCO_2 levels in the phantoms were confirmed with a blood gas analyzer before and after imaging (Radiometer ABL 5).

Mouse Brain pH Measurements. pH sensors (pHOptica) were custom-clad in MRI-compatible PEEK tubing (PlasticsOne) and assembled by World Precision Instruments and PreSens Inc. Sensors were implanted into the amygdala as described (7). Twenty-four hours postimplantation, mice were anesthetized with ketamine/xylazine and imaged on a Varian 4.7-T scanner. CO_2 (10%

and/or 20%) was administered by nasal cannula to lower brain pH as described (7), and $NaHCO_3$ (5 mmol/kg, i.p.) was administered to raise pH as described (7, 29). $T_1\rho$ images were collected by using a fast spin-echo sequence [time to echo (TE) = 12 ms, time to repetition (TR) = 2,000 ms, field of view (FOV) = 30 × 30 mm, imaging matrix size = 256 × 128, slice thickness = 1 mm] with spin-lock durations of 10, 20, 40, and 60 ms and B_1 = 1,000 Hz. $T_1\rho$ maps were generated for each condition, and a 5 × 5 region of interest was placed at the tip of the fiber-optic probe to study the relationship between $T_1\rho$ times and pH measured via the fiber optic sensor.

Functional Brain Imaging (BOLD, $T_1\rho$, and ^{1}H MRS). All human research protocols were approved by the University of Iowa Institutional Review Board. Multimodal functional imaging was performed on six subjects (four males and two females, age 28–35 y). Functional $T_1\rho$ images were collected by using an echo-planar spin-echo sequence (TE = 12 ms, TR = 2,200 ms, FOV = 220 × 220 mm, matrix size = 64 × 64, and slice thickness/gap = 4/1.0 mm) with three spin-lock pulses (10, 30, and 50 ms) and a B_1 frequency of 400 Hz. This sequence had a temporal resolution of 6.6 s per $T_1\rho$ measurement. BOLD imaging was performed by using a T_2* weighted echo-planar gradient-echo sequence (TE = 30 ms, TR = 2,000 ms, FOV = 220 × 220 mm, matrix size = 64 × 64, and slice thickness/gap = 4.0/1.0 mm). For BOLD imaging, seven cycles of flashing checkerboard and visual fixation were presented with an 80-s period. For functional $T_1\rho$ imaging, five cycles were collected with a 72-s period. The ^{1}H MRS data were acquired by using a single-voxel point-resolved spin-echo sequence with water suppression. For functional ^{1}H spectroscopic imaging, the task began in the baseline task followed by the visual activation condition and returning to the baseline condition. For all activation studies, attention was ensured by asking subjects to press a button in response to a red square presented in the center of the screen every 4 s.

All BOLD fMRI data were analyzed by using standard preprocessing steps, including motion correction, slice timing correction, and spatial smoothing. A general linear model was used to generate individual statistical maps and calculate signal change. $T_1\rho$ data were preprocessed by first performing motion correction followed by $T_1\rho$ map generation. $T_1\rho$ data were spatially smoothed, statistical maps were generated by using a general linear model, and estimates of $T_1\rho$ time changes were computed. BOLD percent signal change and $T_1\rho$ time changes were mapped to MNI space where a *t* test was performed across the subjects and corrected for multiple comparisons by using a false discovery rate analysis.

The two ^{1}H spectroscopic measurements obtained for each condition were frequency and phase corrected and averaged, and the resulting spectral data were analyzed by using LCModel. Ratios of Lactate/Cr and Lac/NAA were obtained and compared between (*i*) baseline, (*ii*) activation, and (*iii*) recovery periods using ANOVA.

^{31}P Spectroscopic Functional Measures. Functional data were acquired in six subjects (male/female = 4/2; ages = 22–33 y). A 2D ^{31}P spectroscopic sequence used a free induction decay acquisition (TE = 2.3 ms, TR = 4,000 ms, FOV = 240 × 240 mm, matrix = 8 × 8, thickness = 30 mm, averages = 16, vector size = 1,024). This acquisition was repeated three times (baseline, activation, baseline) with each measurement taking 10 min 24 s. ^{31}P data were analyzed by using the Siemens Syngo software to determine the chemical shift of the inorganic phosphate (Pi) and phosphocreatine (PCr) peaks in the ^{31}P spectra. The analysis included frequency filtering, frequency and phase correction, baseline correction, and curve fitting with prior knowledge. Brain pH was estimated by using the proposed equation (30):

$$\mathrm{pH} = 6.77 + \log\{(\delta - 3.29)/(5.68 - \delta)\},$$

where δ is the chemical shift between in ppm between Pi and PCr. The pH estimates for the baseline, activated, and recovery phases were compared by using ANOVA.

ACKNOWLEDGMENTS. This work was supported by grants from the McKnight Foundation and the Dana Foundation and by a University of Iowa Clinical and Translational Science Award (to V.A.M. and J.A.W.). M.J.W. is an Investigator of the Howard Hughes Medical Institute.

1. Kauppinen RA, Williams SR (1998) Use of NMR spectroscopy in monitoring cerebral pH and metabolism during systemic and focal Acid-Base Disturbances. *pH and Brain Function*, eds Kaila K, Ransom BR (Wiley-Liss, New York), p 605.
2. Esquivel G, Schruers KR, Maddock RJ, Colasanti A, Griez EJ (2010) Acids in the brain: A factor in panic? *J Psychopharmacol* 24:639–647.
3. Chesler M (2003) Regulation and modulation of pH in the brain. *Physiol Rev* 83: 1183–1221.
4. Stewart PA (1978) Independent and dependent variables of acid-base control. *Respir Physiol* 33:9–26.
5. Traynelis SF, Chesler M (2001) Proton release as a modulator of presynaptic function. *Neuron* 32:960–962.
6. Tresguerres M, Buck J, Levin LR (2010) Physiological carbon dioxide, bicarbonate, and pH sensing. *Pflugers Arch* 460:953–964.
7. Ziemann AE, et al. (2009) The amygdala is a chemosensor that detects carbon dioxide and acidosis to elicit fear behavior. *Cell* 139:1012–1021.
8. Wemmie JA, Price MP, Welsh MJ (2006) Acid-sensing ion channels: Advances, questions and therapeutic opportunities. *Trends Neurosci* 29:578–586.
9. Xiong ZG, et al. (2004) Neuroprotection in ischemia: Blocking calcium-permeable acid-sensing ion channels. *Cell* 118:687–698.
10. Friese MA, et al. (2007) Acid-sensing ion channel-1 contributes to axonal degeneration in autoimmune inflammation of the central nervous system. *Nat Med* 13: 1483–1489.
11. Gillies RJ, Raghunand N, Garcia-Martin ML, Gatenby RA (2004) pH imaging. A review of pH measurement methods and applications in cancers. *IEEE Eng Med Biol Mag* 23: 57–64.
12. Mäkelä HI, Gröhn OH, Kettunen MI, Kauppinen RA (2001) Proton exchange as a relaxation mechanism for T1 in the rotating frame in native and immobilized protein solutions. *Biochem Biophys Res Commun* 289:813–818.
13. Zhou J, Payen JF, Wilson DA, Traystman RJ, van Zijl PC (2003) Using the amide proton signals of intracellular proteins and peptides to detect pH effects in MRI. *Nat Med* 9: 1085–1090.
14. Jones CK, et al. (2006) Amide proton transfer imaging of human brain tumors at 3T. *Magn Reson Med* 56:585–592.
15. Jokivarsi KT, et al. (2010) Estimation of the onset time of cerebral ischemia using T1rho and T2 MRI in rats. *Stroke* 41:2335–2340.
16. Kwong KK, et al. (1992) Dynamic magnetic resonance imaging of human brain activity during primary sensory stimulation. *Proc Natl Acad Sci USA* 89:5675–5679.
17. Duvernoy HM, Delon S, Vannson JL (1981) Cortical blood vessels of the human brain. *Brain Res Bull* 7:519–579.
18. Kontos HA, Wei EP, Raper AJ, Patterson JL, Jr. (1977) Local mechanism of CO2 action of cat pial arterioles. *Stroke* 8:226–229.
19. Maddock RJ, Buonocore MH, Copeland LE, Richards AL (2009) Elevated brain lactate responses to neural activation in panic disorder: A dynamic 1H-MRS study. *Mol Psychiatry* 14:537–545.
20. Kaila K, Chesler M (1998) Activity-evoked changes in extracellular pH. *pH and Brain Function*, eds Kaila K, Ransom BR (Wiley-Liss, New York), p 309.
21. Nedergaard M, Goldman SA (1993) Carrier-mediated transport of lactic acid in cultured neurons and astrocytes. *Am J Physiol* 265:R282–R289.
22. Wemmie JA, Zha X, Welsh MJ (2008) Acid-sensing ion channels (ASICs) and pH in synapse physiology. *Structural and Functional Organization of the Synapse*, eds Hell JW, Ehlers MD (Springer, New York).
23. Katsura K, Siesjo B (1998) Acid-base metabolism in ischemia. *pH and Brain Function*, eds Kaila K, Ransom BR (Wiley-Liss, New York), p 563.
24. Siesjö BK, von Hanwehr R, Nergelius G, Nevander G, Ingvar M (1985) Extra- and intracellular pH in the brain during seizures and in the recovery period following the arrest of seizure activity. *J Cereb Blood Flow Metab* 5:47–57.
25. Ziemann AE, et al. (2008) Seizure termination by acidosis depends on ASIC1a. *Nat Neurosci* 11:816–822.
26. Richerson GB (1998) Cellular mechanisms of sensitivity to pH in the mammalian respiratory system. *pH and Brain Function*, eds Kaila K, Ransom BR (Wiley-Liss, New York), pp 509–533.
27. Nattie E, Li A (2009) Central chemoreception is a complex system function that involves multiple brain stem sites. *J Appl Physiol* 106:1464–1466.
28. Friedman SD, Mathis CM, Hayes C, Renshaw P, Dager SR (2006) Brain pH response to hyperventilation in panic disorder: Preliminary evidence for altered acid-base regulation. *Am J Psychiatry* 163:710–715.
29. Schuchmann S, et al. (2006) Experimental febrile seizures are precipitated by a hyperthermia-induced respiratory alkalosis. *Nat Med* 12:817–823.
30. Patel N, Forton DM, Coutts GA, Thomas HC, Taylor-Robinson SD (2000) Intracellular pH measurements of the whole head and the basal ganglia in chronic liver disease: A phosphorus-31 MR spectroscopy study. *Metab Brain Dis* 15:223–240.